High-aspect-ratio microelectromechanical systems deformable mirrors for adaptive optics

Bautista R. Fernández
Joel Kubby
University of California, Santa Cruz
Department of Electrical Engineering
1156 High Street, MS:SOE2
Santa Cruz, California 95064

Abstract. Adaptive optics (AO) applications in astronomy and vision science require deformable mirrors (DMs) with high-stroke, high-order packing density at a lower cost than the currently available technology. The required AO specifications are achievable with microelectromechanical systems (MEMS) devices fabricated with LIGA (lithographie galvanofomung abformung) high-aspect-ratio processing techniques. Different actuator designs and a bonded faceplate fabricated in a LIGA process, enabling multilayer fabrication of MEMS devices, are investigated. Various types of high-stroke gold actuators for AO consisting of folded springs with rectangular and circular membranes as well as x-beam actuators supported diagonally by fixed-guided springs are designed, simulated, and fabricated individually and as part of a continuous-face-sheet DM system. The actuators and DM displacement versus voltage are measured with an interferometer and the corresponding results are compared to finite element analysis simulations. Simulations and interferometer scans show the ability of the actuators to achieve displacements of greater than 1/3 of the initial gap. A stroke of ~9.4 μm is achieved, thus showing that this fabrication process holds promise in the manufacture of future MEMS DMs for the next generation of extremely large telescopes. [DOI: 10.1117/1.3497576]

Subject terms: adaptive optics; large stroke; high aspect ratio; microelectromechanical systems; deformable mirror; electrodeposition; lithographie galvanofomung abformung.

Paper 10019SSPR received Mar. 19, 2010; revised manuscript received Aug. 13, 2010; accepted for publication Aug. 23, 2010; published online Nov. 19, 2010.

1 Introduction

Adaptive optics (AO) is used in astronomy to improve optical image quality by compensating for aberrations caused by fabrication errors, thermal effects, and atmospheric turbulence.[1] The latter is a particularly important aberration when using large astronomical telescopes that see a large part of the sky.

AO systems consist of three primary components: a wavefront sensor, a control system, and a deformable mirror (DM). The DM is used to compensate wavefront errors by rapidly changing its surface geometry. The DM changes the spatial phase of the wavefront with the use of actuators typically placed in a square or hexagonal array that deforms the mirror's surface.[2,3]

For current astronomical applications, the most common DMs use piezoactuators. Future astronomical applications will most likely use microelectromechanical systems (MEMS) due to their lower cost and scalability. Piezo DMs have been created with both segmented and continuous facesheets. Piezoelectric DMs such as lead zirconium titanate (PZT) are fairly large with interactuator spacings of 5 to 10 mm, resulting in large arrays and an increase in the cost and size of the optical system. Each piezoactuator is bonded to a thin reflecting faceplate.[4] A direct current (dc) electric field is applied to the PZT actuators to produce a displacement caused by the piezoelectric effect. Piezoelectric DMs require high voltage and have hystereses of 10 to 20%, causing the displacement of the actuators to be dependent on their past history, making control difficult.[5]

In spite of over a decade of development, current MEMS DMs developed for AO applications in astronomy have not been able to meet the high stroke (10 μm of mechanical displacement) and high order (10,000 actuators) required for future extremely large telescopes such as the Thirty Meter Telescope (TMT), as shown[6] in Table 1.

An even greater stroke, of the order of 15 μm, is required for AO applications in vision science. Current continuous-facesheet MEMS DMs fabricated using surface micromachining processing will require significant process development to meet this specification.[7]

Previous research efforts in MEMS "high-stroke" actuators for DMs have used the Sandia ultraplanar, multilevel MEMS technology[8] (SUMMiT) to fabricate segmented AO mirrors and the MEMSCAP polysilicon surface micromachining process[9] to fabricate continuous-facesheet AO mirrors.[10]

A limitation of MEMS DMs currently fabricated using surface micromachining is the stroke (<6 μm) for continuous-facesheet mirrors. The current commercial MEMS DMs being developed for AO are from Boston Micromachines Corporation[11] (BMC) and IrisAO.[12] BMC can manufacture continuous-facesheet DMs with 300- and 400-μm actuator pitches with a stoke ranging[11] from 1.5 to 5.5 μm and an aperture ranging from 1.5 to ~10 mm. The achievable stroke is limited by the thin-film (2 μm) sacrificial oxide layer used in the surface micromachining process, as shown in Fig. 1(a), that are used to fabricate the mirror [Fig. 1(b)].

1932-5150/2010/$25.00 © 2010 SPIE

Table 1 MEMS DM specifications for the TMT AO system.

Actuator count	4,096 to 10,000 (64×64 and 100×100)
Actuator spacing/clear aperture diameter	400 μm/10 to 40 mm
Stroke range	>10 μm surface
Differential stroke (neighboring actuators)	>1 μm
Bandwidth	>2500 Hz (−3 dB)
Go-to accuracy	<10 nm
Operating temperature	−30°C
Actuator yield	99% [the MCAO (multi conjugate adaptive optics) system; MOAO (multi object adaptive optics) system]; 100% (planet imager)

The layers are deposited using semiconductor thin-film processing. Since the mirror stroke is limited to approximately half the mirror gap by a pull-in instability, which is defined by the sacrificial layer thickness, these actuators have been limited to less than 6 μm of stroke, about half that required for large telescopes. It will be very challenging to modify this process to include sacrificial oxide films that are twice this thickness, as will be required to meet the large-stroke specifications (10 to 15 μm) required for astronomy and vision science applications. A second limitation is that their apertures are too small for many astronomical applications due to the large magnification M required. For a 10-mm-aperture DM used in a 10-m telescope, $M = 10\ \text{m}/10\ \text{mm} = 1000$.

The imagine Optics Mirao 52-e low-order, high-stoke, electromagnetic membrane DM consist of 52 actuators capable of obtaining ± 50 μm of stoke.[13] Each actuator consists of a magnet attached to a thin membrane and induction coils attached to a substrate. A current is applied to the induction coil, which causes a magnetic field that attracts the magnets attached to the membrane. The Mirao 52-e can have an optical coating of aluminum or silver. The mirror's high-order correction is limited by extended deformation of the membrane since the membrane is supported only along its edge, and not by the actuators.

In comparison with the current DMs, the design described in this paper will overcome the limitations in stroke and clear aperture of current continuous-facesheet MEMS DMs and enable both high-stroke and high-order. Unlike current MEMS DMs that are limited in their stroke by the thin (~2 μm) sacrificial layers in the low-aspect-ratio surface micromachining fabrication process, the devices described in this paper were fabricated with a high-aspect ratio LIGA (a German acronym for lithographie, galvanofomung, abformung, meaning lithography, electroforming, molding) process[14] that enables thick material layers (tens to hundreds of micrometers), and thus larger stroke DMs to be fabricated. This will eliminate the need for a woofer-tweeter DM configuration to obtain both high-stroke and high-order correction.[15] A single DM can provide both high-stroke and high-order correction, thus simplifying the design and reducing the overall system cost. The high-aspect-ratio fabrication process is based on patterning thick PMMA (polymethyl-methacrylate) resist films, using synchrotron x-ray radiation.

The PMMA is developed to form a cavity that can be filled with an electroplated metal such as nickel, copper, gold, or a nickel-iron alloy. Electrodeposition is a low-temperature process done in a plating bath that does not require semiconductor thin-film processing or the use of silicon substrates. The process is capable of fabricating structures with high aspect ratios, enabling tall structures to be fabricated to increase the stroke for MEMS DMs, as required for future large-diameter telescopes.

2 Device Design Simulation

Various actuators with assorted spring constants were designed with L-Edit (Tanner EDA, Los Angeles, California) and simulated with finite element analysis (FEA) software[16] (Intellisuite Software, Woburn, Massachusetts).

The actuators that were initially simulated consisted of:

1. a square actuator supported by eight folded springs at the corners
2. a circular actuator supported by folded springs at 90, 180, 270, and 360 deg around its perimeter
3. an x-beam actuator: a square actuator supported diagonally at the corners by fixed-guided beams

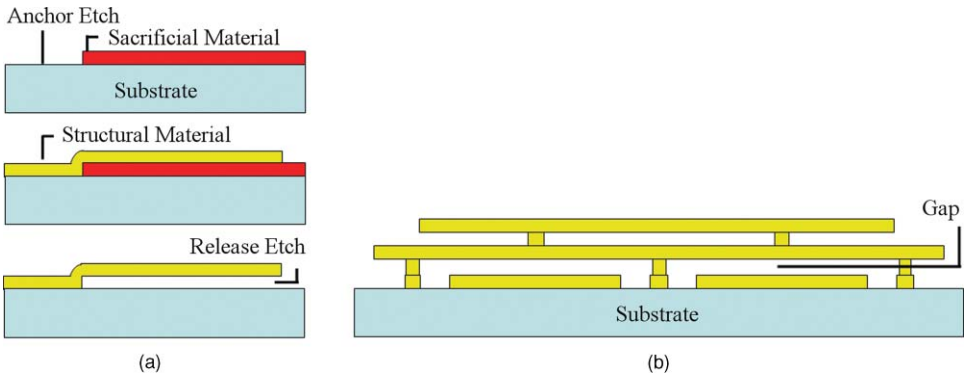

Fig. 1 (a) Generic surface micromachining process and (b) DM created by surface micromachining.

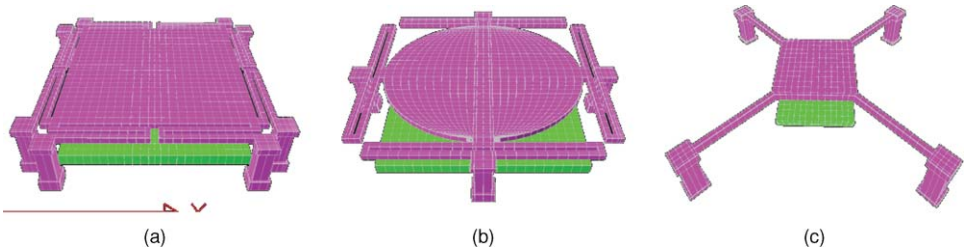

Fig. 2 Three 3-D actuator designs modeled with FEA: (a) square actuators supported by eight folded springs at the corners, (b) circular actuators supported by four folded springs, and (c) x-beam actuators supported by four fixed-guided beams.

The actuator designs that were modeled with FEA are shown in Fig. 2.

All actuators were simulated with gold as the structural material with a tensile stress of 50 MPa. It is important that the center of an actuator displace more than the corners or edges to prevent tilting that can lead to premature pull-in. The folded springs on the eight-corner-spring actuator are meant to help minimize the corners from displacing past the actuator center. Simulations of the eight-corner-spring-support actuator show that it is capable of obtaining a displacement of ~9.8 μm with an applied voltage of 156 V and a corner displacement of 0.9 μm less than the center. A drawback of such a design is that if there are any manufacturing asymmetries, such as layer thickness variations, the stiffness of the springs will not all be the same.

For an ideal situation where the layer thickness is uniform, the pull-in voltage V_{pi} of the actuator supported at the corners by eight folded springs is calculated as follows:

$$k = Ewt^3/L^3 \text{ (spring constant at each corner)}, \quad (1)$$

$$k_{\text{eff}} = 4Ewt^3/L^3 \text{ (spring constant due to four corners)}, \quad (2)$$

$$F_e = 0.5\varepsilon AV^2/(g-\delta)^2 \text{ (electrostatic force)}, \quad (3)$$

$$F_m = k_{\text{eff}}\delta \text{ (mechanical force)}. \quad (4)$$

We can solve for V_{pi} by setting $F_e = F_m$:

$$V_{\text{pi}} = [2k_{\text{eff}}\ \delta(g-\delta)^2/(\varepsilon A)]^{1/2} \text{ (pull-in voltage)}, \quad (5)$$

where $E = 75$ GPa, $w = 20$ μm, $t = 3.5$ μm, $L = 380$ μm, $A = (800\ \mu\text{m})^2$, $g = 32.3$ μm, $\delta = g/3$, and $\varepsilon = 8.85\times10^{-12}$ Fm^{-1}. The values used for the thickness t and the gap g are averaged measurements obtained with a WYKO interferometer. From Eq. (5), the pull-in voltage is ~91 V.

Due to layer thickness variations, the gap and spring layer thickness changes within a distance of 2000 μm by ~0.9 and 0.3 μm, respectively. These thickness changes are the largest measured within the wafer location of the square actuator with eight folded springs in one quadrant of the wafer. The diagonal distance of the corner springs is ~1131 μm with a corresponding spring layer change of 0.2 μm and a gap change of 0.5 μm. The thickness change in the spring layer causes one of the corner spring constants to be different in comparison to the other corners. Although the change is small, the spring constant will vary considerably due to its dependence on t^3. The new corner spring constant will be less stiff:

$$k_{\text{new}} = Ew(t-0.2)^3/L^3 \text{ (spring constant with decrease in thickness)}. \quad (6)$$

This causes a change in the mechanical restoring force. Compared with the other corners, the mechanical force of this corner has changed by $\sim1.9\times10^{-6}$ N, which is a ~16.2% decrease. The corner with the slightly smaller gap also experiences a larger electrostatic force applied to it, causing the corner to displace farther than the other corners. This causes the mirror to tilt rather than translate vertically, leading to premature pull-in.

To prevent the premature pull-in attributed to the uneven displacement of the corners of the square actuators, a circular actuator was designed. The circular actuator was capable of obtaining a displacement of ~9.9 μm with an applied voltage of 167 V. The perimeter of the circular actuator was displaced by 0.7 μm less than the center. One drawback of such an actuator is the increase in the voltage required to displace it by 10 μm, due to the smaller electrode area. To minimize tilting it is necessary to constrain the top electrode of the actuators more rigidly. One way to achieve this is to support

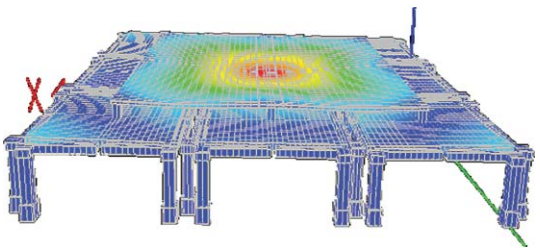

Fig. 3 FEA simulation of a mirror system consisting of square actuators with a 30-μm gap supported by eight corner springs.

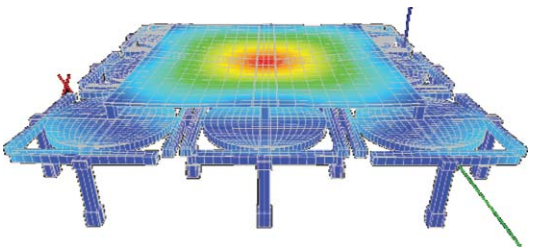

Fig. 4 FEA simulation of mirror system consisting of circular actuators with a 30-μm gap supported by four folded springs.

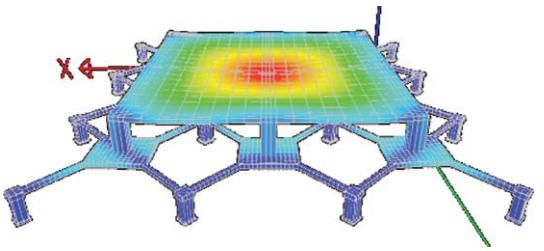

Fig. 5 FEA simulation of mirror system consisting of x-beam actuators with a 20-μm gap supported by four fixed-guided beams.

a rectangular actuator at the corners by fixed-guided beams, such as the x-beam actuator shown in Fig. 2(c).

The center square electrode in the x-beam actuator measures 400×400 μm with four 390- × 20-μm fixed-guided beams. The x-beam actuator's fixed-guided beams become nonlinear when displaced by more than half of the spring layer thickness, thus allowing the mechanical "strain stiffening" effect to increase the actuators travel range to more than half the gap.[17] The increased travel range allows an actuator with a 20-μm gap to achieve a 10-μm stoke. The x-beam actuator design helped minimize the tilting associated with gap and spring thickness variations. A drawback of the x-beam actuators is the large voltage (280 V based on FEA) required to achieve a displacement of ~10 μm. The springs can be described with the nonlinear spring equation:[18]

$$F_m = k_1'\delta + k_s'\delta^3 \text{ (nonlinear spring equation)}, \quad (7)$$

$$k_1 = 16Ewt^3/L^3 \text{ (linear spring constant for fixed-fixed beam)}, \quad (8)$$

$$k_1' = 32Ewt^3/L^3 \text{ (linear spring constant assuming two fixed-fixed beams)}, \quad (9)$$

$$k_s = \pi^4 Ewt/(8L^3) \text{ (nonlinear stretching component)}, \quad (10)$$

$$k_s' = \pi^4 Ewt/(4L^3) \text{ (nonlinear stretching component for two springs)}. \quad (11)$$

By equating Eqs. (3) and (7) the pull-in voltage is found:

$$V_{\text{pi}} = (2(k_1'\delta + k_s'\delta^3)(g-\delta)^2/(\varepsilon A))^{1/2} \text{ (pull-in voltage)}, \quad (12)$$

where: $E = 75$ GPa, $w = 20$ μm, $t = 5$ μm, $L = 780$ μm, $A = (400\ \mu\text{m})^2$, $g = 20$ μm, $\delta = 10$ μm, and $\varepsilon = 8.85\times 10^{-12}$ Fm^{-1}. From Eq. (12), the pull-in voltage is 269 V. Ignoring the nonlinear spring component $k_s\delta^3$ the pull-in voltage is 134 V. The spring constant increases from ~126 (linear) to ~511 μN/m (nonlinear).

The individual actuators were also simulated as part of a mirror system composed of an array of 3×3 actuators. The center actuator in the 3×3 mirror system was actuated by approximately 10 μm, as shown in Figs. 3, 4, and 5. The surrounding eight actuators were grounded and act as spring supports.

The boundary condition was a mirror membrane supported by posts attached to the top of the actuators. This type of boundary condition enables the edge of the mirror to move with the actuators supporting it. Simulation of this type of boundary condition in conjunction with either the actuators supported at the corners with eight springs or the circular actuators showed that the difference in height between the center and edge of the actuators was smaller than 0.5 μm when displaced to ~10 μm. Figure 3 shows a side view of the simulated mirror system with eight corner-spring-support actuators.

For the mirror system with eight corner-spring actuators with a 30-μm gap, a center displacement of 9.9 μm at 190 V is expected. The difference between the center and the corners was ~0.4 μm. When modeling with the circular actuators with a 30-μm gap, a 9.9-μm displacement is achieved at 202 V. The difference from the perimeter of the actuator to its center was ~0.1 μm. Figure 4 shows a side view of the simulated mirror system with circular actuators.

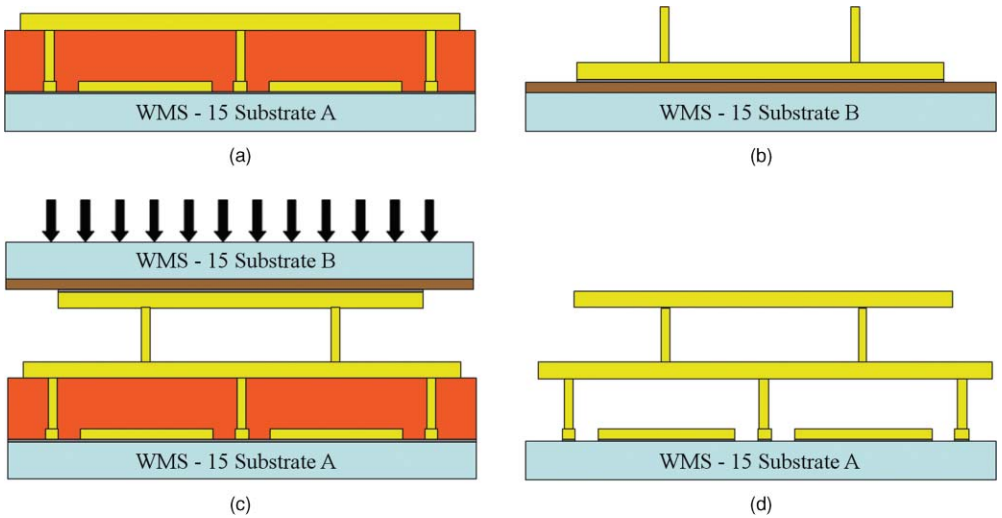

Fig. 6 General fabrication process example: (a) wafer A for fabrication of actuators, (b) wafer B for fabrication of facesheet, (c) bonding wafer B to wafer A, and (d) release structures by removal of wafer B and sacrificial material.

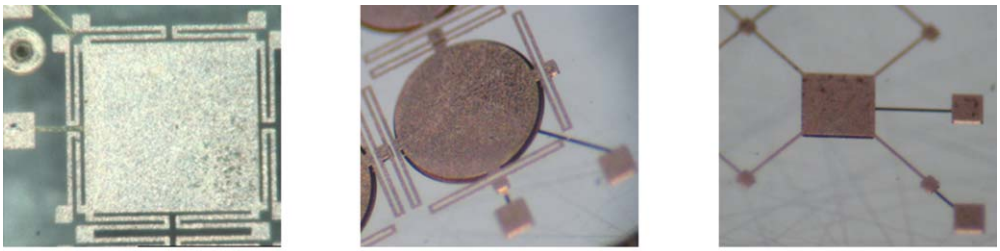

Fig. 7 Fabricated gold actuators: (a) square actuators supported by eight folded springs at the corners, (b) circular actuators supported by four folded springs, and (c) x-beam actuators supported by four fixed-guided beams.

The simulation of the x-beam actuator with the same boundary condition, showed a displacement of ~ 10 μm at a voltage of 322 V. Since the device is supported at the corners diagonally, tilting is minimized. The nonlinear spring constant also provides feedback to stabilize tilting. If a corner tilts down, the beam is stretched, making it stiffer. Figure 5 shows a side view of the simulated mirror system with x-beam actuators.

3 Device Fabrication

DMs consisting of the actuators shown in Fig. 2 were fabricated with a high-aspect-ratio LIGA process (HT MicroAnalytical, Albuquerque, New Mexico). The fabrication of the deformable mirror is a two-wafer bonding process. Both wafers are optically flat glass-ceramic substrates that are used to make wavelength division multiplexing filters in the telecommunications industry [<1 nm root mean square (rms) roughness] that have a closely matched coefficient of thermal expansion (CTE) of 11.4×10^{-6} K^{-1} to the electroplated gold structural layers with a CTE of 14.2×10^{-6} K^{-1}.

On the first wafer (substrate A), the fabrication process begins with deposition of a plating base (chrome/titanium) on its surface that will enable the structural layer (gold) and sacrificial material (copper) to be electroplated, as shown in Fig. 6(a). The facesheet is fabricated on the second wafer (substrate B). A ProLIFT^{TM} (Brewer Science, Rolla, Missouri) release layer is deposited on the wafer surface followed by a plating base layer. The ProLIFT^{TM} release layer is intended to enable easy removal of the wafer from the facesheet. The facesheet is patterned in a thick photoresist and then electroplated through the photoresist mask, followed by patterning and electroplating of the support post. To ensure that all the posts are of equal height, a planarization step is performed.

Once both substrates A and B are fabricated, as shown in Figs. 6(a) and 6(b), the next step is to align the substrates and bond substrate B onto substrate A, as shown in Fig. 6(c). The bonding of the substrates is performed at a temperature of 225°C for 4 h using a constant pressure of 40 MPa. After bonding has been achieved, the next step is to release the fabricated structure. The release of the electroplated structures starts by removing substrate B, by chemically removing the ProLIFT^{TM} layer and the remaining plating base. The final step consists of removing the sacrificial material (copper) from substrate A and any remaining plating base. Figure 6(d) shows the released faceplate attached to actuators.

Utilizing the fabrication process described previously for Fig. 6(a), different actuators were fabricated out of gold, as shown in Fig. 7. Due to the size and shape of the actuator's folded springs and to manufacturing asymmetries, the tilting of the actuators shown in Figs. 7(a) and 7(b) occurred. Development of an x-beam actuator [Fig. 7(c)] was undertaken to prevent this unwanted behavior before reaching the desired 10 μm of stroke. The fabrication was performed on a 4-in. glass-ceramic wafer that was divided into four quadrants ($Q1$, $Q2$, $Q3$, and $Q4$), which were individually characterized as described in the following section.

An example of a facesheet bonded to actuators is shown in Fig. 8. Here, the face sheet is bonded to an array of x-beam actuators. Only a corner of the mirror is within the field of view. The mirror was tilted up to show the actuators located below the face sheet.

4 Device Testing

4.1 *Actuator Testing*

Fabrication metrology was conducted with a white light interferometer (WYKO NT1100). Bow-tie[19] test structures with vernier scales were analyzed to determine the residual stress and multi-layer alignment structures were measured to determined layer thicknesses. Measurement of the bow-tie vernier displacement revealed that stress varied over the four quadrants of the wafer. The following stresses for the wafer quadrants were found: $Q1 = 69$ MPa, $Q2 = 72$ MPa, $Q3 = 70$ MPa, and $Q4 = 51$ MPa. The average tensile stress measured across the wafer was 66 MPa with a standard deviation of 9.8 MPa. From the multilayer alignment test structures it was determined that the average separator (gap) and spring layers thickness varied by 0.2 μm and that there was a 10-μm misalignment in the x direction. The misalignment was negligible in the y direction. Figure 9 shows a visual

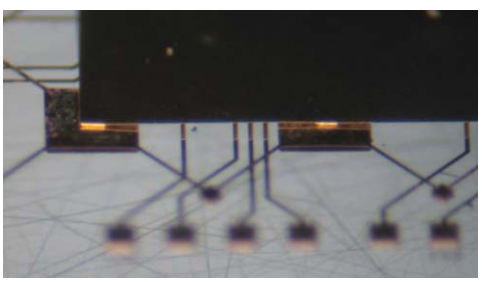

Fig. 8 Facesheet bonded to an array of x-beam actuators.

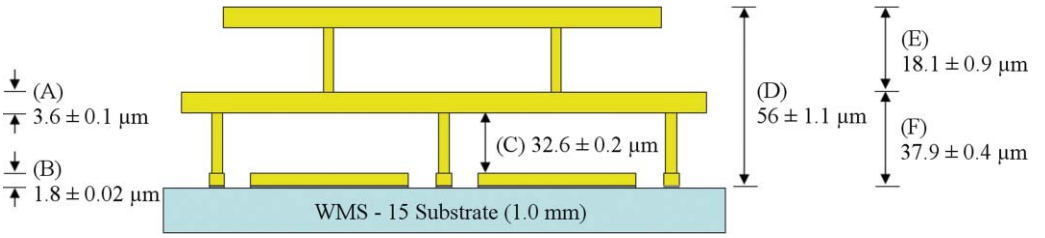

Fig. 9 Average measured layer thickness.

representation of the layer thicknesses. The average stress and layer thicknesses measured were used to model the actuators with FEA.

A 200-V power supply was used to test the actuators and displacement versus voltage scans were obtained with the interferometer. The displacement results from modeling were compared to the displacements measured with the interferometer scans for the fabricated devices. For the displacement comparisons, the actuators were not actuated to the full design goal of 10 μm to prevent the device from pulling-in. These designs (except for the x-beam actuator) tend to tilt as they translate vertically, resulting in pull-in at a smaller displacement than predicted by the modeling results, which predict only the vertical translation. The tilting of the actuators results from small manufacturing asymmetries in the fabricated devices. For this reason the x-beam design, which is more robust to tilting, is preferred. Results comparing the simulations to actual interferometer results are shown in Figs. 10 and 11.

From the comparison plots, we can see that the results are in agreement with the simulations obtained utilizing FEA at a low voltage and deviate at higher voltages near the predicted pull-in. The deviation is due to tilting of the actuators during testing rather than the pure vertical translation as assumed in the modeling results.

Some of the actuators were tested until pull-in occurred to determine if the actuators would snap-in uniformly. Based on this snap-in test it was determined that the square actuators had a tendency to pull-in at a corner first, whereas the circular actuators would tilt diagonally between the springs. This snap-in phenomenon, along with the interferometer scans, helped to determine that these two actuators tilt as they are being actuated. Although this tilting will be constrained once a faceplate is attached, the tilt could add additional deformation to the DM faceplate and could also lead to premature pull-in.

A white light interferometer scan of an x-beam actuator without a facesheet attached revealed that the initial height of the fabricated x-beam actuator was greater than designed. Hence a gap size of ~28.5 μm was obtained instead of the 20-μm gap for which this particular fabrication run was designed. The average thickness of the spring layer was ~3.5 μm instead of the 5-μm thickness in the design. This larger gap increased the voltage required to actuate the device and achieve ~10 μm of stroke. A voltage of 377 V was required to displace ~9.3 μm. Figure 12 shows an interferometer scan of a x-beam actuator displaced by ~9.3 μm.

4.2 *DM Testing*

Results were obtained for the displacement versus voltage of a small 2×2 DM array consisting of a square actuator supported at the corners by two U-shaped folded springs. A displacement of ~9.4 μm was measured using a white-light interferometer. Hence, our high-precision fabrication process holds promise for fabricating MEMS DMs for the next generation of extremely large telescopes. Unlike other MEMS technologies, this device has a large displacement, a continuous facesheet (membrane), and is made of gold. Given that the DM is made of gold, there is no need for a protective window, as is used in current MEMS DMs fabricated from polysilicon. Protective windows help prevent oxidation from occurring on polysilicon structures.[20] While protective windows can have an antireflective coating deposited, they limit the spectral range since they work over only a narrow bandwidth.

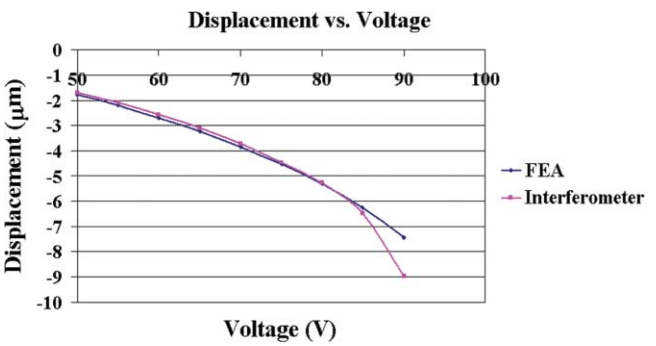

Fig. 10 Comparison of displacement versus voltage for a square actuator supported at the corners; interferometer scan versus FEA.

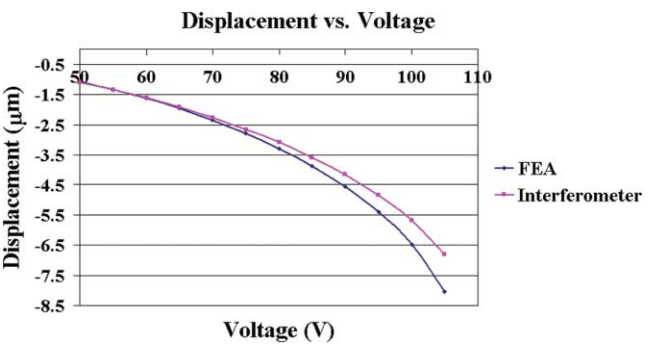

Fig. 11 Comparison of displacement versus voltage for a circular actuator supported by folded springs; interferometer scan versus FEA.

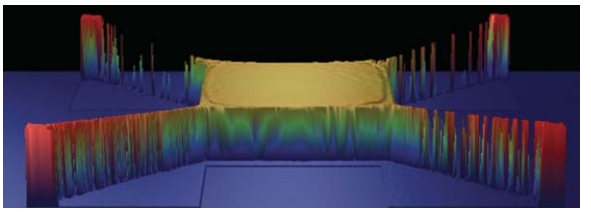

Fig. 12 Interferometer scan of an x-beam actuator displaced by ~9.3 μm.

5 Conclusions

Different gold actuators were designed, simulated, and fabricated with a high-aspect-ratio LIGA process that enabled large displacements to be obtained. A displacement of ~9.4 μm was also achieved with a 2×2 DM consisting of a continuous-facesheet membrane attached to eight corner-spring actuators. We also determined that the eight corner-spring and circular actuators tend to tilt as they are being actuated, which can lead to premature pull-in. This tilting was addressed with the design of the x-beam actuator supported diagonally by fixed-guided beams.

Acknowledgments

This work was supported in part by the National Science Foundation Science & Technology Center for Adaptive Optics, managed by the University of California at Santa Cruz under Cooperative Agreement No. AST-9876783. The authors would like to acknowledge the contributions of Jeff Sniegowski and Todd Christenson at HT MicroAnalytical, Inc., for adapting their high-aspect-ratio LIGA process to our deformable mirror designs.

References

1. R. K. Tyson, *Adaptive Optics Engineering Handbook*, Marcel Dekker, New York (2000).
2. T. G. Bifano, J. Perreault, R. K. Mali, and M. N. Horenstein, "Microelectromechanical deformable mirrors," *Journal of Selected Topics in Quantum Electronics* **5**, 83–90 (1999).
3. C. L. Hom, P. D. Dean, and S. R. Winzer, "Modeling electrostrictive deformable mirrors in adaptive optics systems," *Proc. SPIE* **3985**, 394–405 (2000).
4. F. Roddier, *Adaptive Optics in Astronomy*, Cambridge University Press, New York (1999).
5. J. W. Hardy, *Adaptive Optics for Astronomical Telescopes*, Oxford University Press, New York (1998).
6. D. Gavel, "MEMS for the next generation of giant astronomical telescopes," in *MEMS/MOEMS Components and Their Applications III*, S. S. Olivier, S. A. Tadigadapa, and A. K. Henning, *Proc. SPIE* **6113**, 611307 (2006).
7. B. Fernandez and J. Kubby, "Design, processing and materials for large-stroke actuators," *Proc. SPIE* **6467**, 64670 T (2007).
8. J. J. Allen, *Micro Electro Mechanical System Design*, pp. 88–94, CRC Press, Boca Raton, FL (2005).
9. J. M. Bustillo, R. T. Howe, and R. S. Muller, "Surface micromachining for microelectromechanical systems," *Proc. IEEE* **86**, 1552–1574 (1998).
10. P. Krulevitch, "MOEMS spatial light modulator development at the Center for Adaptive Optics," in *MOEMS and Miniaturized Systems III, Proc. SPIE* **4983**, 227–233 (2003).
11. T. Bifano, P. Bierden, and J. Perreault, "Micromachined deformable mirrors for dynamic wavefront control," *Proc. SPIE* **5553**, 10–13 (2004).
12. M. A. Helmbrecht, T. Juneau, M. Hart, and N. Doble, "Performance of a high-stroke segmented MEMS deformable-mirror technology," *Proc. SPIE* **6113**, 611330 L (2006).
13. N. Savage, "Adaptive optics," *Nature Photonics* **2**, 756–757 (2008).
14. T. Christenson, "X-ray-based-fabrication," Chap. 18 in *The MEMS Handbook*, pp. 18-1–18-46 CRC Press, Boca Raton, FL (2002).
15. K. Morzinski, B. Macintosh, D. Gavel, and D. Dillon, "Stroke saturation on a MEMS deformable mirror for woofer-tweeter adaptive optics," *Optics Express* **17**, 5829–5843 (2009).
16. B. Fernandez and J. Kubby, "Simulation and interferometer results of MEMS deformable mirrors," *Proc. SPIE* **6888**, 68880R (2008).
17. E. S. Hung and S. D. Senturia, "Extending the travel range of analog-tuned electrostatic actuators," *Journal of Microelectromechanical Systems* **8**, 497–505 (1999).
18. G. M. Rebeiz, *RF MEMS: Theory, Design, and Technology*, pp. 21–58, Wiley, New York (2003).
19. Y. B. Gianchandani and K. Najafi, "Bent-beam strain Sensors," *Journal of Microelectromechanical Systems* **5**, 52–58 (1996).
20. H. R. Shea, A. Gasparyan, H. B. Chan, S. Arney, R. E. Frahm, D. Lopez, S. Jin, and P. P. McConnell, "Effects of electrical leakage currents on MEMS reliability and performance," *IEEE Transactions on Device Material Reliability* **4**, 198–207 (2004).

Bautista R. Fernández is a PhD candidate in electrical engineering at the University of California, Santa Cruz, with a concentration in microelectromechanical systems (MEMS) with applications in adaptive optics. He received his BS and MS degrees in electrical engineering from the University of California, Santa Cruz, in 2004 and 2007, respectively.

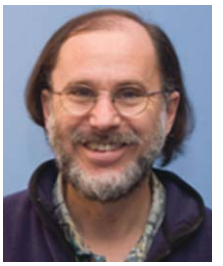

Joel Kubby is an associate professor of electrical engineering with the Baskin School of Engineering at the University of California, Santa Cruz. His research is in the area of microelectromechanical systems (MEMS) with applications in optics, fluidics, and bio-MEMS. Prior to joining the University of California, Santa Cruz, in 2005, he was a manager with the Xerox Wilson Center for Research and Technology and a member of the technical staff of the Webster Research Center in Rochester New York from 1987 to 2005. Prior to Xerox he was with the Bell Telephone Laboratories in Murray Hill, New Jersey, working in the area of scanning tunneling microscopy (STM). He received his PhD degree in applied physics from Cornell University and his BA degree in physics from the University of California, Berkeley. He is the cochair of the SPIE Silicon Photonics Conference and the MEMS Adaptive Optics Conference.